ASTRONOMY & ASTROPHYSICS
SUPPLEMENT SERIES

Astron. Astrophys. Suppl. Ser. **132**, 197–210 (1998)

Optical colour maps of Seyfert galaxies

II. More Seyfert 2s⋆

J.K. Kotilainen[1,2]

[1] International School for Advanced Studies (SISSA), via Beirut 2–4, I–34014 Trieste, Italy
[2] Tuorla Observatory, University of Turku, Väisäläntie 20, FIN–21500 Piikkiö, Finland
e-mail: jarkot@deneb.astro.utu.fi

Received January 30; accepted April 20, 1998

Abstract. We present optical broad band $B - I$ colour maps of a further sample of 10 Seyfert 2 galaxies. In these bands, the contribution from emission lines to the total flux is small, and hence the images predominantly trace the continuum distribution. As in our earlier colour maps of a sample of Seyferts type 1 and 2, we detect extended blue continuum components in the circumnuclear region of several galaxies. These components are either elongated (in Mkn 533, Mkn 607, Mkn 1066, NGC 5347, NGC 5953 and NGC 7319) or form a double structure across the nucleus (in NGC 5929). They are closely aligned with the radio and emission line axes of these galaxies and probably arise from scattering of nuclear continuum light by extranuclear mirrors. Similar blue elongations (in Mkn 1 and NGC 7212) and double structures (in NGC 788) are less well aligned with the radio and line emission, and their relationship with scattering regions must be considered uncertain. The colours of the blue maxima are consistent with those expected from scattering off dust or electrons, a conclusion strengthened by the combined sample of the two papers in this series. Our findings thus strongly support the current unified models of AGN.

Key words: galaxies: active — galaxies: nuclei — galaxies: seyfert — galaxies: stellar content — galaxies: structure

Send offprint requests to: J.K. Kotilainen (Tuorla address)

⋆ Based on observations made with the Nordic Optical Telescope, operated on the island of La Palma jointly by Denmark, Finland, Iceland, Norway, and Sweden, in the Spanish Observatorio del Roque de los Muchachos of the Instituto de Astrofisica de Canarias.

1. Introduction

In the unified models of active galactic nuclei (AGN), the observed differences between various types of AGN are explained in terms of collimated radiation, obscuration and viewing angle effects on intrinsically similar objects (e.g. Antonucci 1993). Specifically for Seyfert galaxies, there is increasing evidence (for references see Sect. 4 and Kotilainen & Ward 1997; hereafter KW97), that in Seyfert 2s optically thick material, in the form of a thick disk or a dusty torus, blocks our direct view of the compact nucleus and the broad line region (BLR), and collimates the ionising photons along the minor axis of the torus into two oppositely directed cones.

The emphasis in studies of the nuclear regions of Seyferts has been on the emission line properties (e.g. integral field spectroscopy and emission line imaging). However, although the nuclear torus is expected to be too small to be resolved, its outer parts, e.g. in the form of a flattened red dust distribution, may be detectable in continuum colour maps. Evidence for these obscuring regions, perpendicular to the bipolar extended narrow line region (ENLR) has been detected in e.g. NGC 5252 (Tadhunter & Tsvetanov 1989; Kotilainen & Prieto 1995) and Mkn 348 (Simpson et al. 1996). Similarly, continuum colour maps have revealed blue morphological features coincident with the high-excitation gas in the ENLR (e.g. Pogge & De Robertis 1993, 1995; Mulchaey et al. 1996a; KW97). In KW97, we presented high resolution colour maps of three Seyfert 1 and six Seyfert 2 galaxies. These maps revealed the existence of blue elongations and double structures in NGC 1068, NGC 3227, NGC 4151, Mkn 3 and Mkn 573, that were not discernible in single filter images, and that we interpreted as scattered nuclear light. In this paper, we present similar colour maps of the circumnuclear regions of 10 more Seyfert 2 galaxies. We briefly describe the observations, data reduction and the methods used in the construction of the colour maps in Sect. 2. In Sect. 3 we

Table 1. The colours of the blue maxima, their distance from the nuclei, and the relevant position angles

Galaxy	FWHM arcsec	PA(°) ([OIII])	PA(°) (radio)	PA (°) $(B-I)$	$D(''$)	D(kpc)	$B-V$	$V-R$	$V-I$
(1)	(2)	(3)	(4)	(5)	(6)	(7)	(8)	(9)	(10)
Mkn 1	0.8	83		290	2.5	1.2	0.47	0.19	0.42
Mkn 533	0.8		117	310	3.2	2.7	0.99	0.32	0.75
Mkn 607	0.6	132		320	0.9	0.23	1.02	0.55	1.30
Mkn 1066	0.6	131	134	325	4.2	1.5	0.92	0.80	1.50
NGC 788	0.7	105		315	1.1	0.43	1.01	0.49	1.13
				170	0.4	0.15	1.10	0.55	1.21
NGC 5347	0.8	0		10	2.6	0.60	0.69	0.51	1.18
NGC 5929	0.7	60	61	45	2.0	0.50	0.94	0.74	1.53
				225	0.8	0.20	0.99	0.86	1.38
NGC 5953	0.7	50	40	220	0.5	0.10	1.04	0.78	1.16
NGC 7212	0.7	10		165	0.4	0.31	1.35	0.23	0.68
				165	1.8	1.4	1.14	0.22	0.68
NGC 7319	0.8	202	207	10	1.1	0.72	1.29	0.74	1.46

present and discuss the morphological features detected for each galaxy, including comparison with available multiwavelength data. In Sect. 4 we discuss the relevance of our findings in the enlarged sample of Seyfert galaxies, in view of current unified AGN models. Conclusions are presented in Sect. 5. Throughout this paper we use Hubble constant $H_0 = 50$ km s^{-1} Mpc^{-1}, and deceleration parameter $q_0 = 0$.

2. Observations, data reduction and construction of the colour maps

The galaxies were observed through broad band B, V, R and I filters, as a part of our study of the integrated properties of the host galaxies of Seyfert 2 nuclei (Kotilainen 1998). We used the BroCam 1024^2 px CCD camera with pixel scale $0.176''$ px^{-1} at the Cassegrain focus of the 2.5 m Nordic Optical Telescope (NOT) on La Palma, in August 1995 and July 1996. Conditions were photometric throughout with generally subarcsec seeing. The images were reduced with standard procedures, i.e. bias subtraction, flatfielding, residual sky subtraction, and removal of cosmic rays and bad pixels. Multiple exposures were coadded after accurate alignment to produce the final images. Photometric calibration was obtained against faint standard stars selected from Landolt (1992). Airmass correction was applied using extinction coefficients appropriate for La Palma. We estimate the internal statistical errors from the standard star observations to be ± 0.03 mag. For further information and for photometry of the galaxies, see Kotilainen (1998).

Colour maps were produced from the B and I band images smoothed to the same (lower) resolution, after careful alignment using the centroids of the light distribution of field stars as reference points. Misalignments of only a small fraction of a pixel may remain, and they do not affect the results for structures covering a large number of pixels. The images were smoothed with a Gaussian filter with a width corresponding to the seeing, and the I band image was divided by the B band image. In the resulting logarithmic colour maps, dark shades indicate blue and light shades red emission. At the edge of the colour maps noise dominates, but closer to the nucleus the colours are reliable. To check that the detected structures in the colour maps are not artifacts caused by e.g. variable seeing or alignment errors, we have inspected the colour residuals of field stars. Reassuringly, they do not show any artifacts but cancel out well in the colour maps. Another problem is the contamination from emission lines within the broad bands. As discussed in KW97, while the V and R filters are severely affected by emission lines, the B and I filters are practically devoid of strong emission lines, and are dominated by continuum emission. This conclusion is supported by a literature search of equivalent widths (EW) of major optical emission lines in the nuclear spectra of the sample galaxies. The average contribution of emission lines to the B and I filters in this sample are 6% and 4%, respectively. In the next section, we present and discuss for each galaxy a direct B band image for morphological information and $B-I$ colour maps (Figs. 1–26).

3. Results

3.1. Mkn 1

Mkn 1 (NGC 449) is a highly inclined SB0a galaxy at redshift $z = 0.0159$, with $1''$ corresponding to 460 pc projected distance in the sky. We show its B band image in Fig. 1. The [OIII] emission has radial extent $\sim 9''$ (4 kpc) at PA = 83°, elongated along the major axis of the nuclear continuum at PA = 87° (Mulchaey & Wilson 1995).

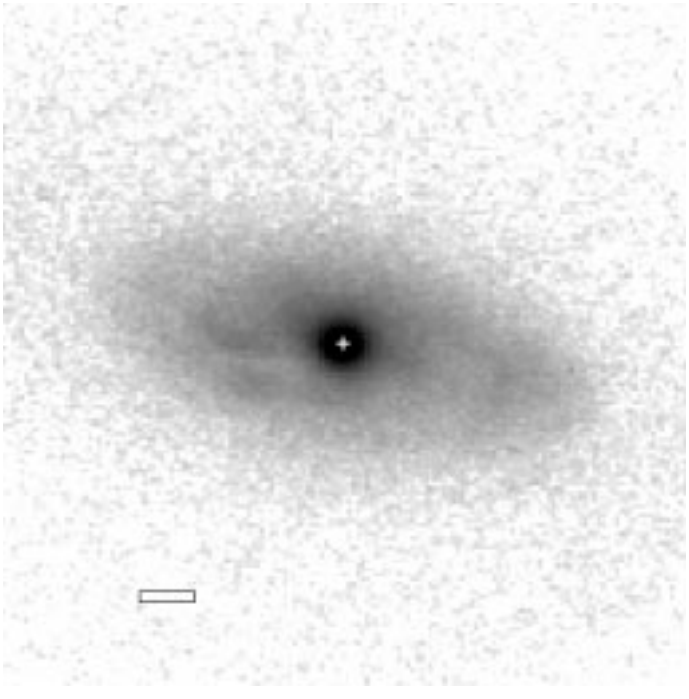

Fig. 1. The B band image of Mkn 1. The size of the image is $26 \times 26''$ (12×12 kpc). In this and other figures, north is up, east to the left, the nucleus of the Seyfert galaxy is marked as a cross and, unless otherwise indicated, the scale bar corresponds to 1 kpc projected distance in the sky

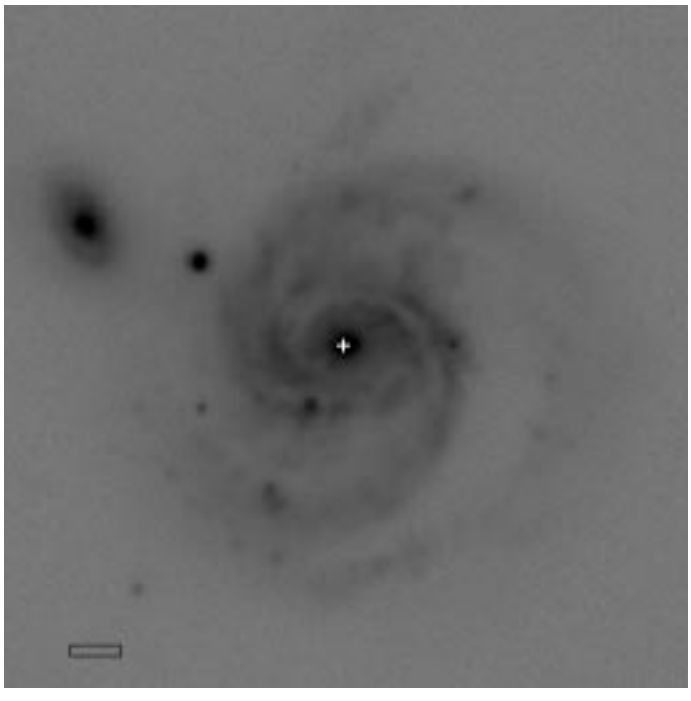

Fig. 3. The B band image of Mkn 533. The size of the image is $79 \times 79''$ (67×67 kpc). The scale bar corresponds to 5 kpc projected distance in the sky

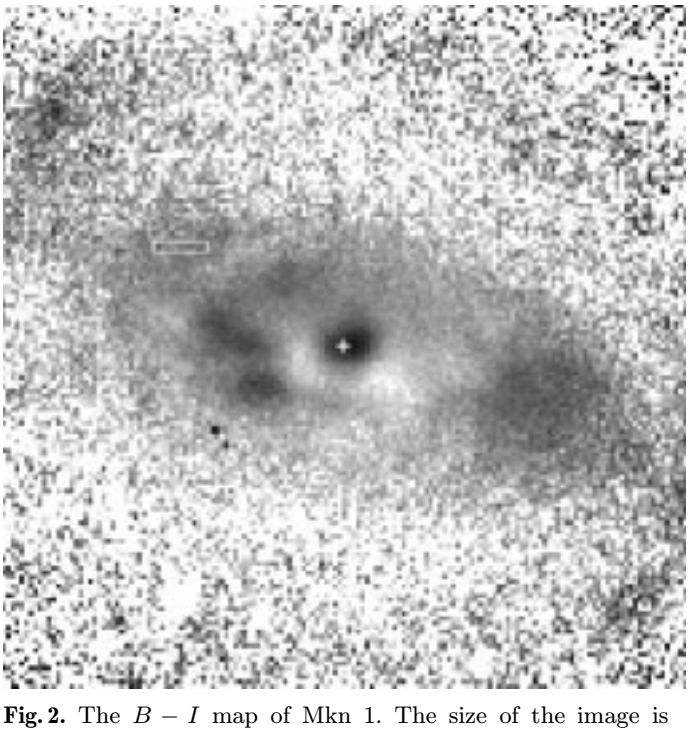

Fig. 2. The $B - I$ map of Mkn 1. The size of the image is $26 \times 26''$ (12×12 kpc). In this and other colour maps, dark shades indicate blue and light shades red emission. The $B - I$ colour coding is from 1.0 to 2.0. Note the blue elongation across the nucleus at PA = 290° of $\sim 2.5''$ (1.2 kpc) extent

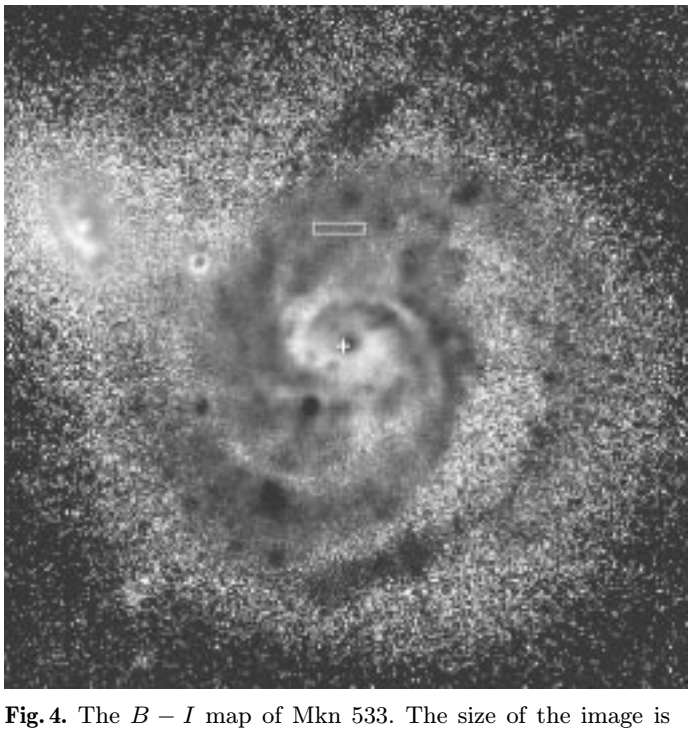

Fig. 4. The $B - I$ map of Mkn 533. The size of the image is $79 \times 79''$ (67×67 kpc). The $B-I$ colour coding is from 1.2 to 2.4. The scale bar corresponds to 5 kpc projected distance in the sky. Spiral structure and star forming regions are clearly visible in the main body of the galaxy. There is a blue elongation with a total extent of $3.2''$ (2.7 kpc) from the nucleus along PA = 310°

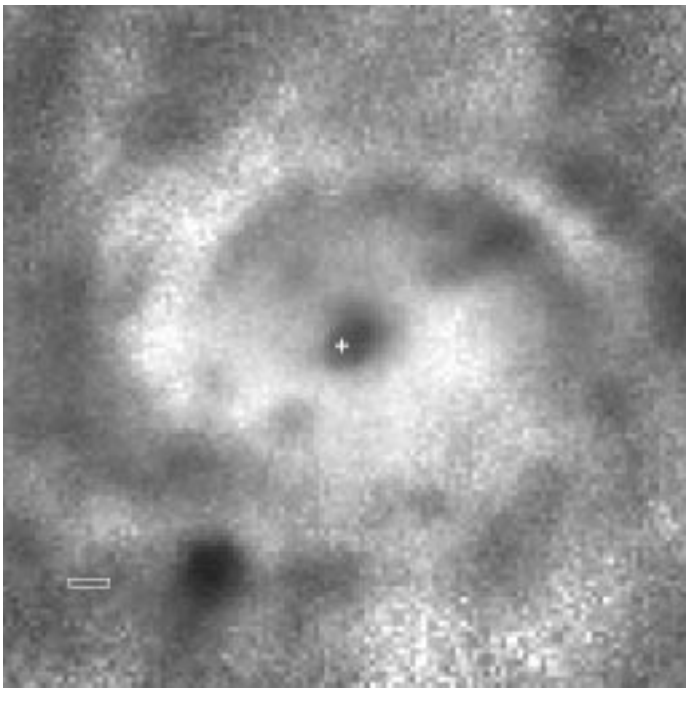

Fig. 5. The $B-I$ map of the innermost $21 \times 21''$ (18×18 kpc) of Mkn 533, showing more clearly the structures seen in Fig. 4. The $B-I$ colour coding is from 0.7 to 2.4

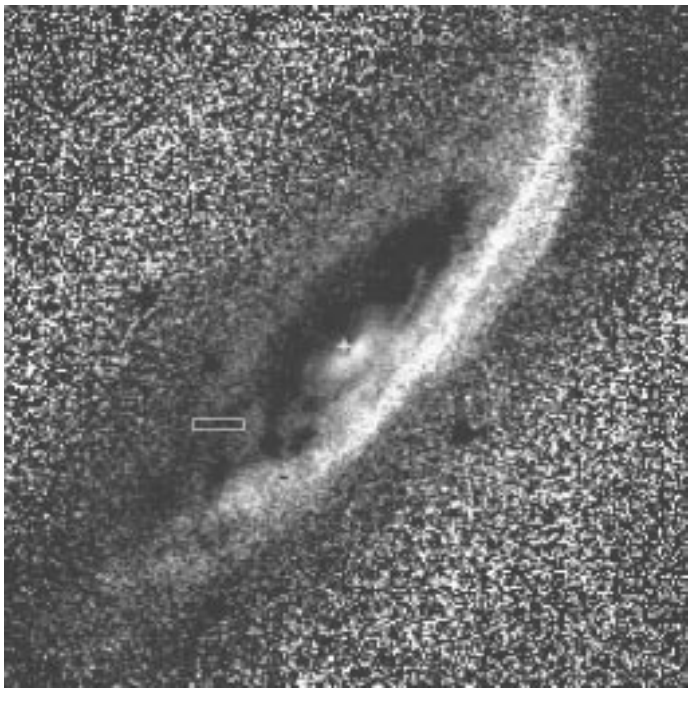

Fig. 7. The $B-I$ map of Mkn 607. The size of the image is $53 \times 53''$ (14×14 kpc). The $B-I$ colour coding is from 2.2 to 2.8. Note the red dust lane along the whole SW side of the galaxy. Star forming regions are visible in the main body of the galaxy

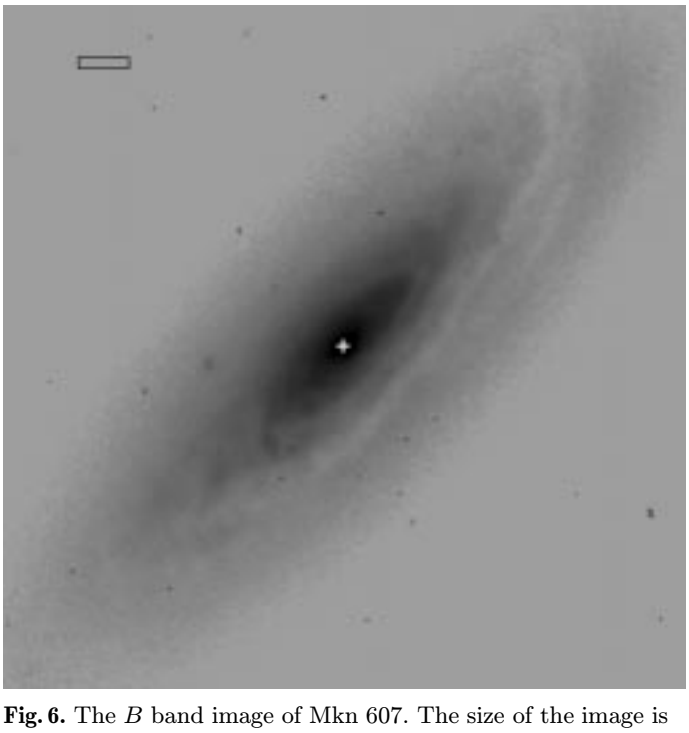

Fig. 6. The B band image of Mkn 607. The size of the image is $53 \times 53''$ (14×14 kpc)

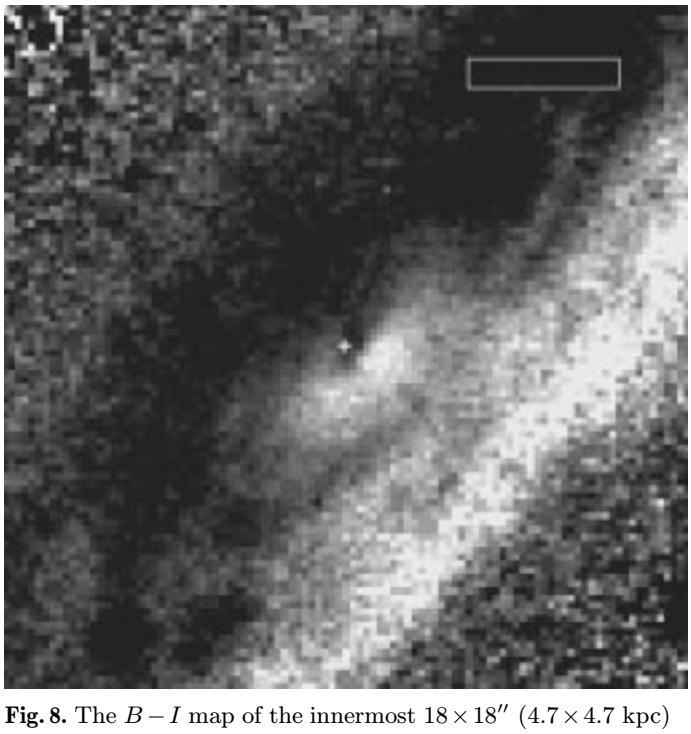

Fig. 8. The $B-I$ map of the innermost $18 \times 18''$ (4.7×4.7 kpc) of Mkn 607. The $B-I$ colour coding is from 2.2 to 2.8. Note the possible blue elongation emanating at PA $= 320^\circ$ up to $0.9''$ (230 pc) distance from the nucleus. There is a red region on the SW side of the nucleus, probably related to the larger scale dust lane (Fig. 7)

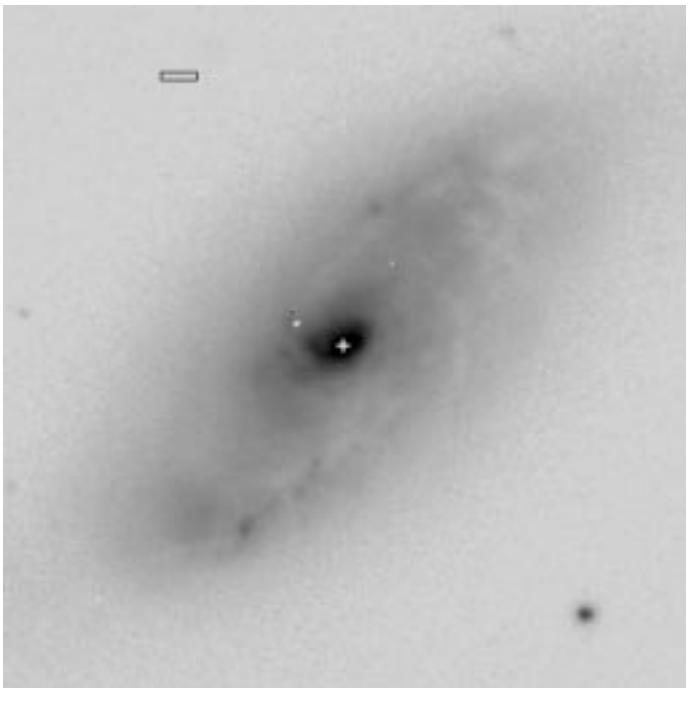

Fig. 9. The B band image of Mkn 1066. The size of the image is $53 \times 53''$ (19×19 kpc)

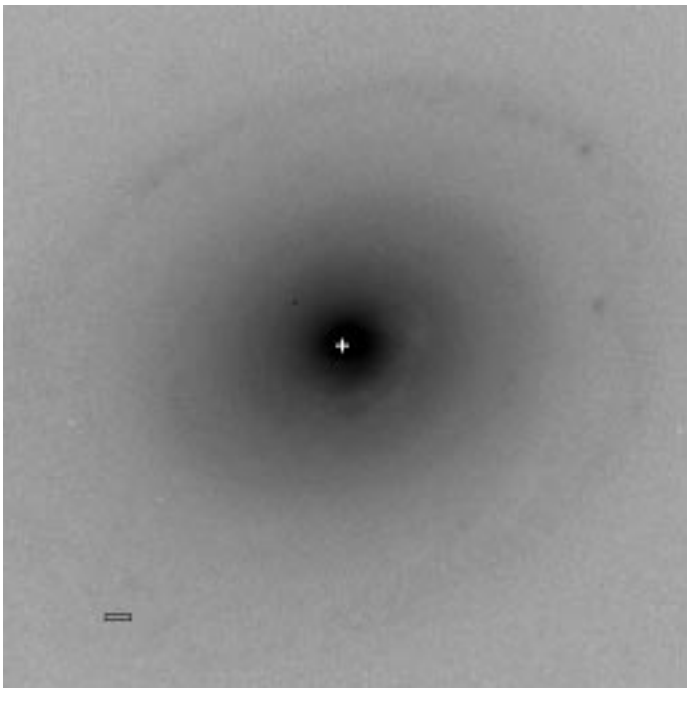

Fig. 11. The B band image of NGC 788. The size of the image is $70 \times 70''$ (27×27 kpc)

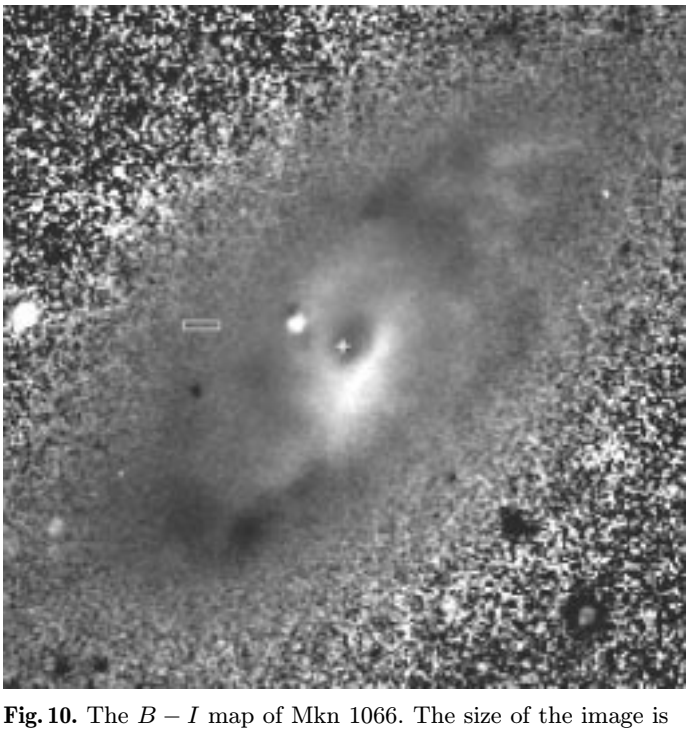

Fig. 10. The $B - I$ map of Mkn 1066. The size of the image is $53 \times 53''$ (19×19 kpc). The $B - I$ colour coding is from 1.6 to 3.0. Note that the I band image is saturated in the nucleus, so the structure in the central few pixels is not real. There is a blue elongated region at PA = 326° from the nucleus with $2.6''$ (910 pc) extent, and a very red region SW of the nucleus. Spiral arms and star forming regions are visible in the disk

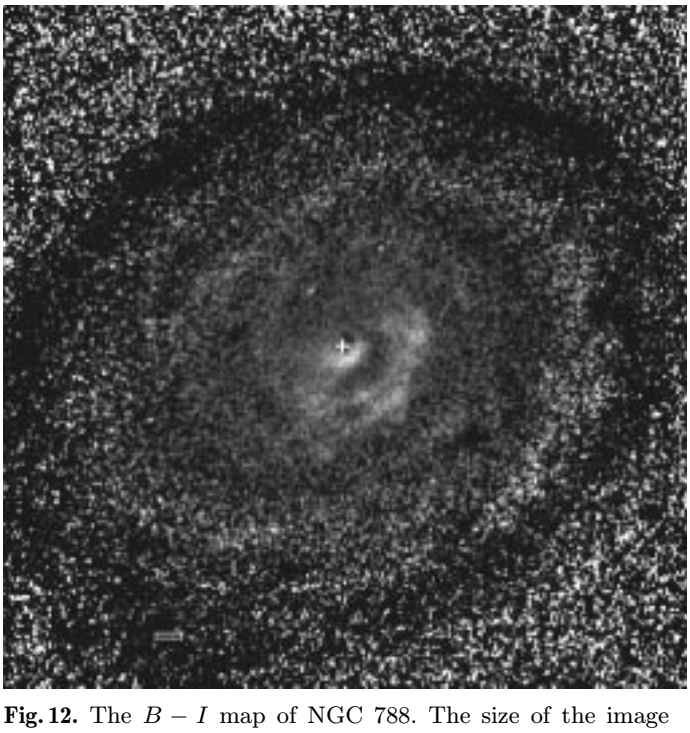

Fig. 12. The $B - I$ map of NGC 788. The size of the image is $70 \times 70''$ (27×27 kpc). The $B - I$ colour coding is from 2.2 to 2.6. Note the blue inclined ring of emission at $\sim 30''$ (12 kpc) radius from the nucleus (see also Fig. 11). The nucleus is situated between two blue regions, at $0.4''$ (150 pc) along PA = 170° and at $1.1''$ (430 pc) along PA = 316°. There is also an extended red region SW of the nucleus

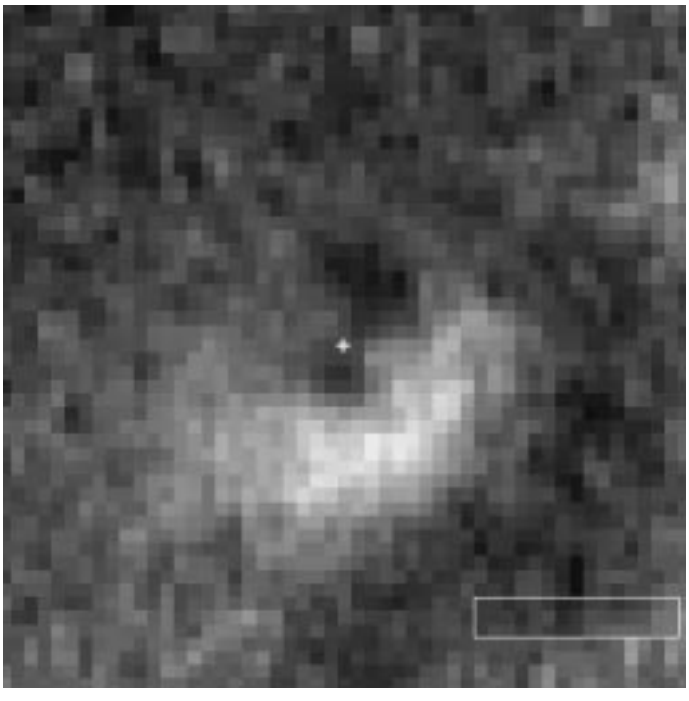

Fig. 13. The $B-I$ map of the innermost $8.8\times8.8''$ (3.4×3.4 kpc) of NGC 788, showing more clearly the structures seen in Fig. 12. The $B-I$ colour coding is from 2.2 to 2.6

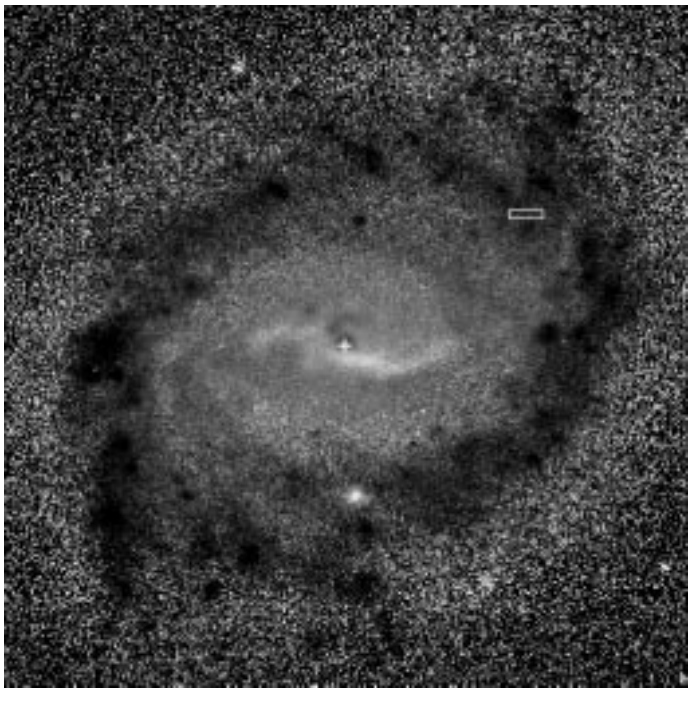

Fig. 15. The $B-I$ map of NGC 5347. The size of the image is $88\times88''$ (20×20 kpc). The $B-I$ colour coding is from 0.7 to 2.1. Note the red dust lane running S of the nucleus roughly from E to W, probably related to the bar, and a blue elongation of $\sim2.6''$ (600 pc) extent N of the nucleus at PA $= 8^\circ$

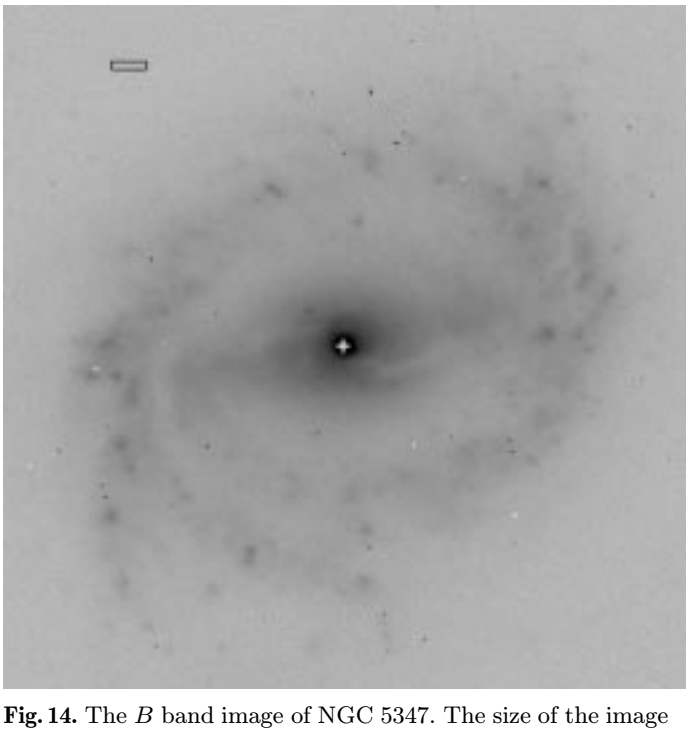

Fig. 14. The B band image of NGC 5347. The size of the image is $88\times88''$ (20×20 kpc)

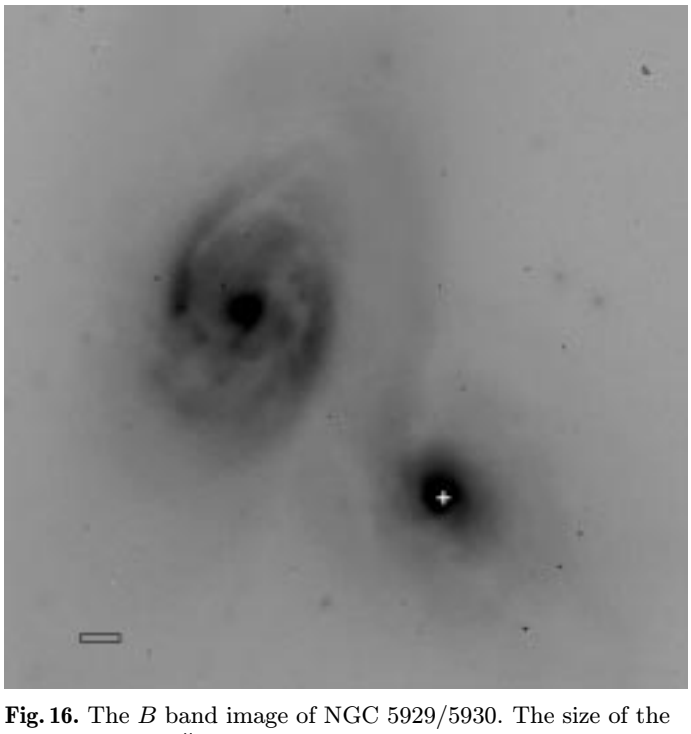

Fig. 16. The B band image of NGC 5929/5930. The size of the image is $70\times70''$ (18×18 kpc). NGC 5929 is situated in the SW and NGC 5930 in the NE part of the figure

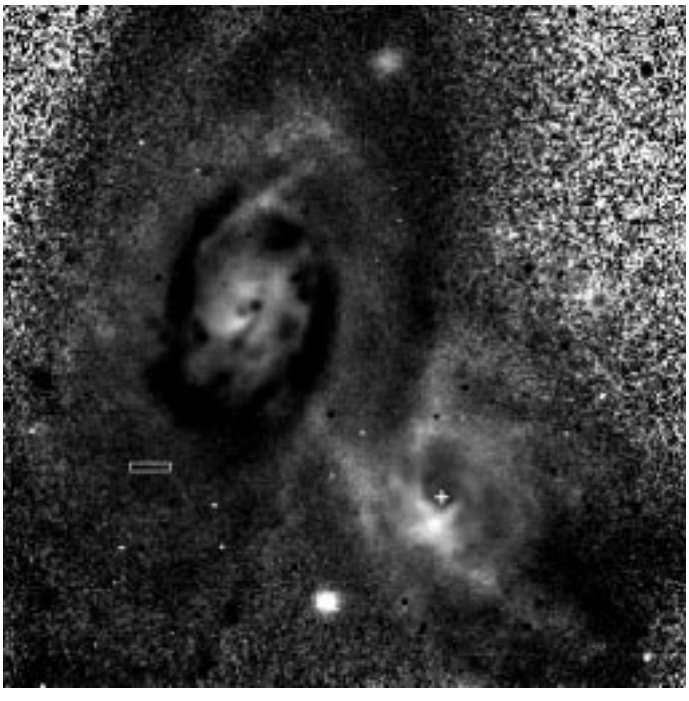

Fig. 17. The $B-I$ map of NGC 5929/5930. The size of the image is $70 \times 70''$ (18×18 kpc). The $B-I$ colour coding is from 1.0 to 2.4. NGC 5929 is situated in the SW and NGC 5930 in the NE part of the figure. The blue stellar tail from the N part of NGC 5929 toward NGC 5930 and the red stellar bridge between the galaxies are clearly visible. The nuclear region of NGC 5929 has double blue peaks at opposite sides of the nucleus, at $0.8''$ (200 pc) at PA $= 227°$, and at $2.0''$ (500 pc) at PA $= 47°$). There is also a very red region S of the nucleus

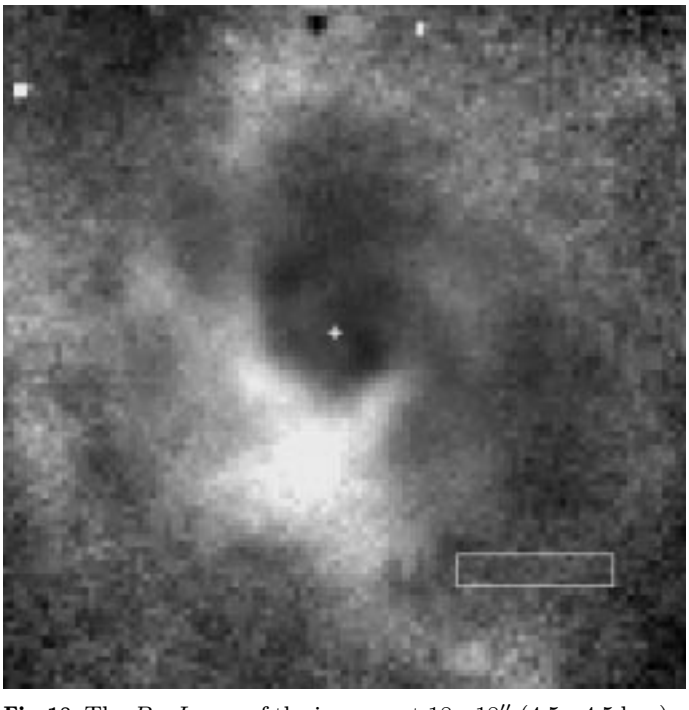

Fig. 18. The $B-I$ map of the innermost $18 \times 18''$ (4.5×4.5 kpc) of NGC 5929, showing more clearly the structures seen in Fig. 17. The $B-I$ colour coding is from 1.0 to 2.3

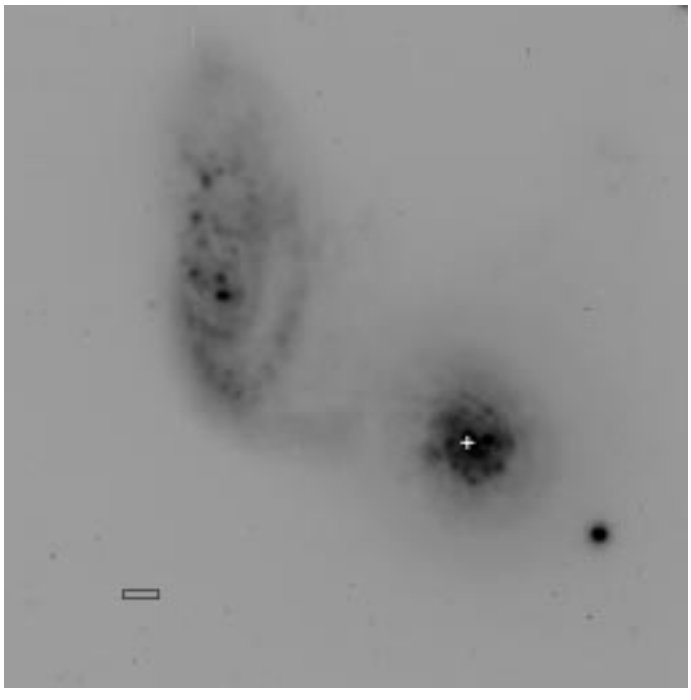

Fig. 19. The B band image of NGC 5953/5954. The size of the image is $106 \times 106''$ (20×20 kpc). NGC 5953 is situated in the SW and NGC 5954 in the NE part of the figure

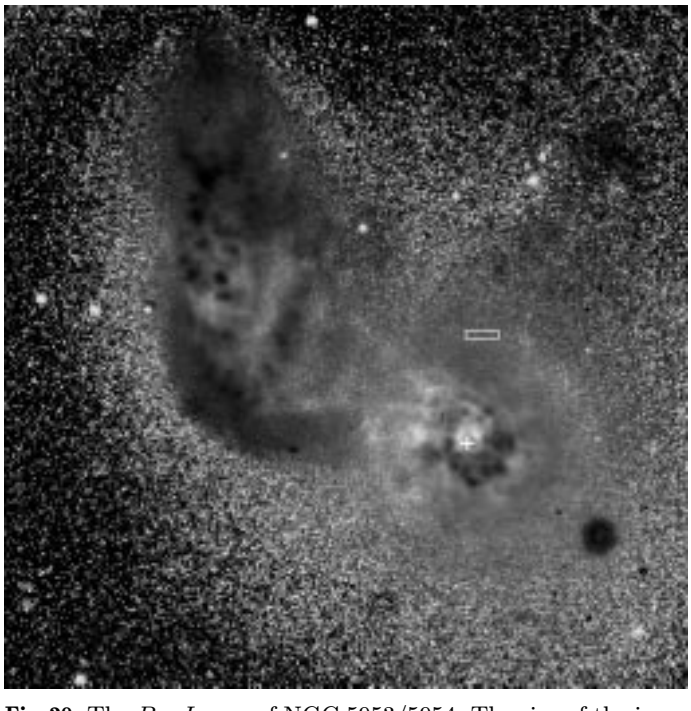

Fig. 20. The $B-I$ map of NGC 5953/5954. The size of the image is $106 \times 106''$ (20×20 kpc). The $B-I$ colour coding is from 0.2 to 2.2. NGC 5953 is situated in the SW and NGC 5954 in the NE part of the figure. Note the blue stellar bridge between the galaxies, and the long plume of blue emission NW of NGC 5953. There is a red arc around the nucleus of NGC 5953 E–N–W, and an inclined lopsided star forming ring roughly N–S with diameter $13 \times 8''$ (2.5×1.5 kpc). Finally, there is possibly a blue elongated structure up to $0.5''$ (100 pc) from the nucleus at PA $= 221°$

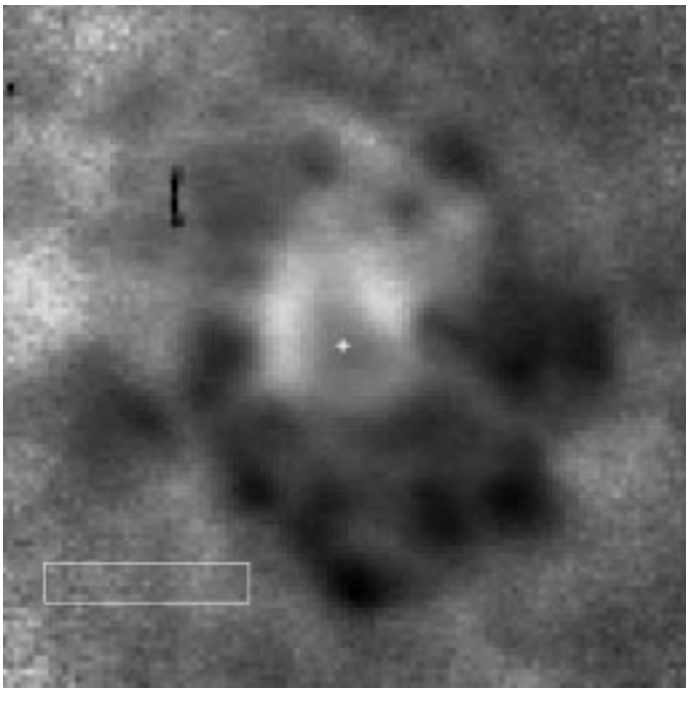

Fig. 21. The $B-I$ map of the innermost $18\times18''$ (3.4×3.4 kpc) of NGC 5953, showing more clearly the structures seen in Fig. 20. The $B-I$ colour coding is from 0.7 to 2.2

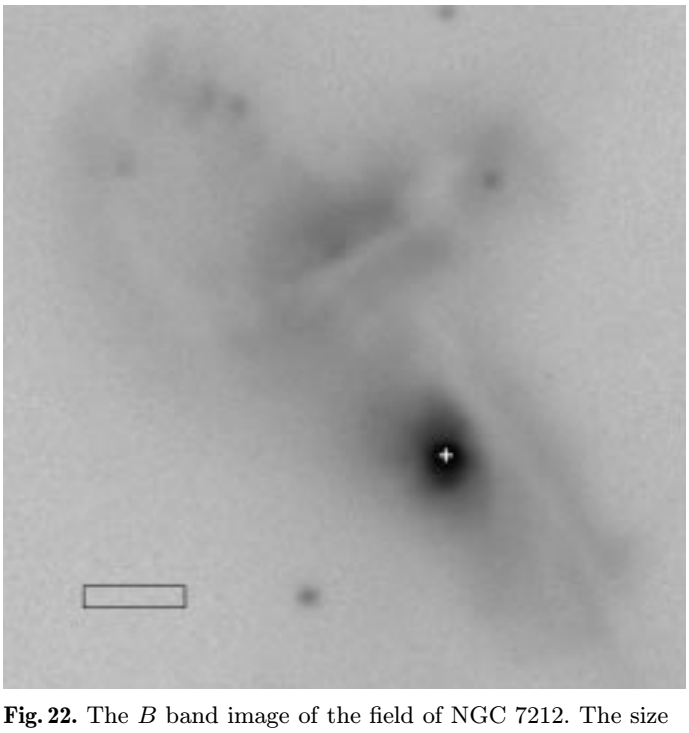

Fig. 22. The B band image of the field of NGC 7212. The size of the image is $44\times44''$ (34×34 kpc). NGC 7212 is situated in the SW and the main companion galaxy in the NE part of the figure. The scale bar corresponds to 5 kpc projected distance in the sky

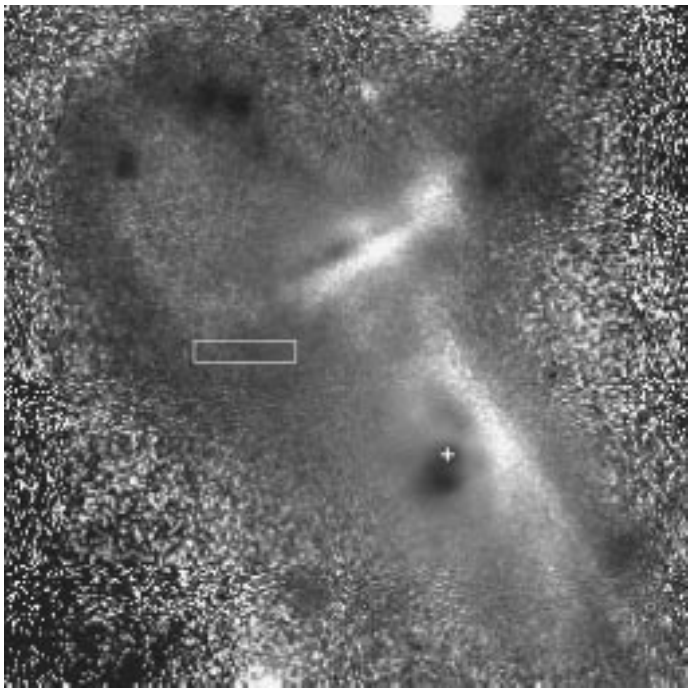

Fig. 23. The $B-I$ map of the field of NGC 7212. The size of the image is $44\times44''$ (34×34 kpc). The $B-I$ colour coding is from 1.4 to 3.1. NGC 7212 is situated in the SW and the main companion galaxy in the NE part of the figure. The scale bar corresponds to 5 kpc projected distance in the sky. The nuclear region of NGC 7212 is very blue and an extended fan–shaped blue region emanates from the nucleus along PA $= 166^\circ$, with total extent of $2.3''$ (1.8 kpc). This blue region is bisected by a red dust lane. A red narrow dust lane is visible on the other side of the nucleus

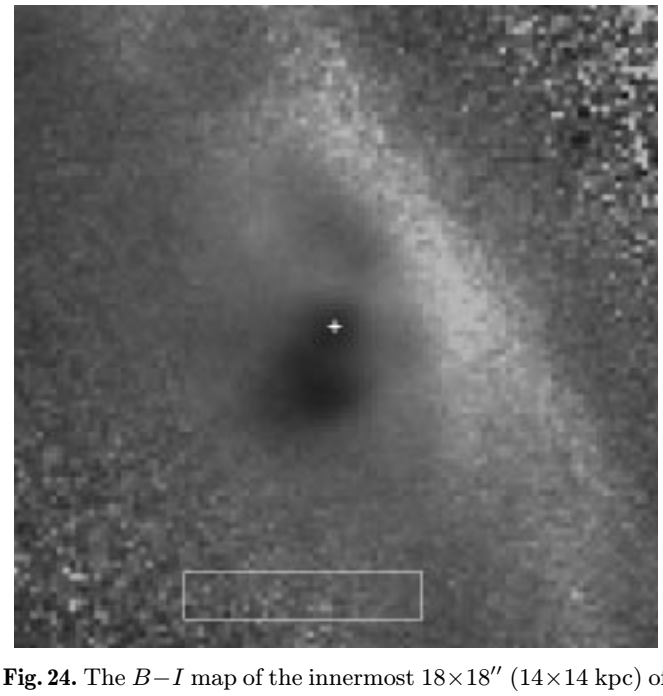

Fig. 24. The $B-I$ map of the innermost $18\times18''$ (14×14 kpc) of NGC 7212, showing more clearly the structures seen in Fig. 23. The $B-I$ colour coding is from 1.4 to 3.1. The scale bar corresponds to 5 kpc projected distance in the sky

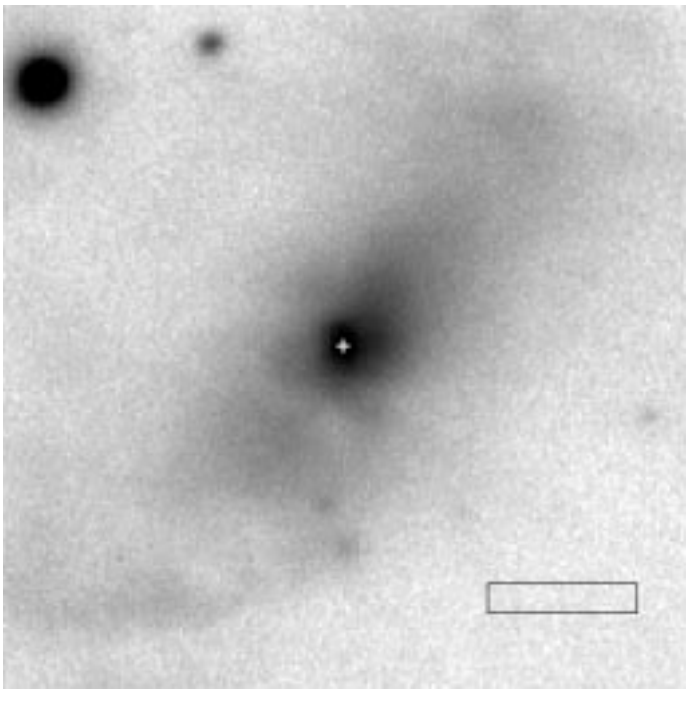

Fig. 25. The B band image of NGC 7319. The size of the image is $35 \times 35''$ (23×23 kpc). The scale bar corresponds to 5 kpc projected distance in the sky

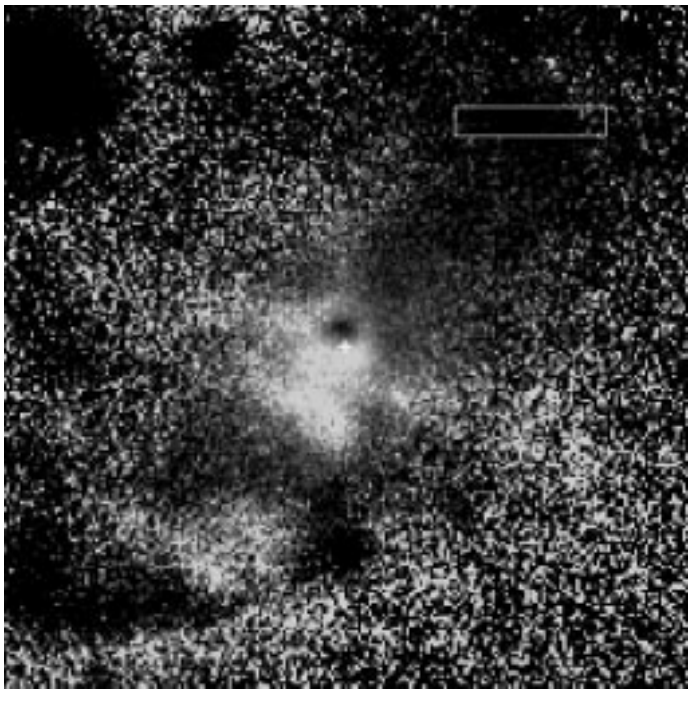

Fig. 26. The $B - I$ map of NGC 7319. The size of the image is $35 \times 35''$ (23×23 kpc). The $B - I$ colour coding is from 2.4 to 3.0. The scale bar corresponds to 5 kpc projected distance in the sky. The bluest region lies at $1.1''$ (720 pc) from the nucleus at PA $= 10°$. To the S of the nucleus at $0.7''$ (460 pc) there is a very red region, extending further S as a red region

Although the profiles of optical emission lines of Mkn 1 show blue asymmetry (e.g. De Robertis & Shaw 1990), no asymmetry or evident broad wings are seen in the near–infrared (NIR; Veilleux et al. 1997). There is, therefore, no strong evidence for an obscured BLR in Mkn 1.

We show the $B - I$ map of Mkn 1 in Fig. 2. There are several blue regions in the host galaxy to the E and SE of the nucleus, probably related to star forming activity, and an arclike red region situated S of the nucleus. Closer to the center, there is a blue elongated structure of $\sim 2.5''$ (1.2 kpc extent across the nucleus at PA $= 290°$). The nucleus is slightly closer to the E end of this elongation. Although not closely parallel to the axis of the [OIII] emission (PA $= 83°$; Mulchaey & Wilson 1995), this blue elongation may be caused by scattered light from the nucleus. We shall discuss the origin of the detected structures in all the galaxies, in the context of the unified models, in Sect. 4. The colours of the blue elongation are given in Table 1. Note that in all the galaxies studied, these colours include a contribution from the red underlying stellar population in the nuclear region. Therefore, the real colours of the structures must be even bluer than those reported here.

3.2. Mkn 533

Mkn 533 (NGC 7674, Arp 182) is an SBb spiral galaxy at $z = 0.0289$, with $1''$ corresponding to 840 pc projected distance in sky. We show the B band image of Mkn 533 in Fig. 3. It has asymmetric arms and tidal connection to the nearby compact elliptical, NGC 7675. Mkn 533 has a nuclear double radio source, with diameter $\sim 0.75''$ (630 pc) at PA $= 117°$ (Kukula et al. 1995). Hα emission of Mkn 533 has polarised broad wings (Miller & Goodrich 1990; Tran 1995a; Young et al. 1996). The nuclear polarisation rises steeply to the blue, the polarised flux spectrum is much bluer than the total flux spectrum, and the polarisation PA $\sim 31°$ is independent of wavelength, and perpendicular to the radio axis. All this indicates dust scattering as the main polarisation mechanism.

The forbidden optical emission lines (e.g. [OIII]) in Mkn 533 have strong blue wings (e.g. De Robertis & Shaw 1990; Veilleux 1991) and broad wings have been found in the NIR HeI, Paβ and Brγ lines (Ruiz et al. 1994; Veilleux et al. 1997). Further evidence for an obscured central source in Mkn 533 comes from the hard X-ray spectrum, which shows a prominent Fe K line and a flat powerlaw continuum, well fitted by a steep intrinsic spectrum reflected by optically thick cold matter (Malaguti et al. 1998). The intrinsic X-ray luminosity is at least one order of magnitude larger than what is observed.

We present the $B - I$ maps of Mkn 533 in Fig. 4 (the whole galaxy) and Fig. 5 (nuclear region). The spiral structure, effects of dust reddening and star forming regions are clearly visible in the disk of Mkn 533 (Fig. 4). In the nuclear region (Fig. 5), there is a blue elongation from the

nucleus to NW (PA = 310°) of 3.2″ (2.7 kpc) total extent. This structure is aligned closely parallel to the radio axis and perpendicular to the polarisation orientation, and probably represents scattered light from the nucleus. Its colours are given in Table 1.

3.3. Mkn 607

Mkn 607 (NGC 1320) is a nearly edge–on S0a galaxy at redshift $z = 0.0090$, with 1″ corresponding to 260 pc projected distance in the sky. We show a B band image of Mkn 607 in Fig. 6. The [OIII] emission is extended along the major axis of the host galaxy (PA = 137°) with ∼12″ (3.1 kpc) radius (Mulchaey et al. 1996b). The PA of the innermost [OIII] emission and that of the nuclear continuum emission is 132° (Mulchaey & Wilson 1995; Mulchaey et al. 1996b).

We show the $B - I$ maps of Mkn 607 in Fig. 7 (the whole galaxy) and Fig. 8 (nuclear region). A red narrow dust lane at closest distance of 5.1″ (1.3 kpc) is visible along the whole SW side of the host galaxy (already seen in the B band image; Fig. 6). Several blue star forming regions can be detected in the host galaxy (Fig. 7). In the central region (Fig. 8), a red extended region is visible on the SW side of the nucleus (at 1.2″; 310 pc), probably related to the larger scale SW dust lane. In addition, there is a faint blue elongated structure emanating from the nucleus toward NW (PA = 320°) up to 0.9″ (230 pc) distance. Its orientation agrees perfectly with the axis of the [OIII] emission, and possibly represents scattered light from the nucleus. Its colours are given in Table 1.

3.4. Mkn 1066

Mkn 1066 (UGC 2456) is an inclined SB(s)0 galaxy at redshift $z = 0.0121$, with 1″ corresponding to 350 pc projected distance on the sky. We show its B band image in Fig. 9. The nuclear continuum is aligned at PA = 137° (Mulchaey et al. 1996b). The radial extent of the [OIII] emission is 6.5″ (2.3 kpc) at PA = 134°, with a double structure across the nucleus separated by ∼3.3″ (1.2 kpc) at PA = 131° (Mulchaey et al. 1996b). The innermost [OIII] gas is concentrated into a narrow jet–like feature extending 1.4″ (490 pc) NW of the nucleus at PA ∼ 310°, with much fainter emission up to 0.8″ (280 pc) SE at PA ∼ 130° (Bower et al. 1995). The [OIII] emission is thus parallel to the axis of the linear triple radio source extending 2.8″ (1.0 kpc) with bipolar jetlike morphology along PA = 134° (Ulvestad & Wilson 1989). No polarised or NIR broad lines have been detected in Mkn 1066 (Miller & Goodrich 1990; Kay 1994; Veilleux et al. 1997), and the UV continuum polarisation is parallel to the radio axis, unlike in the Seyfert 2s with evidence for scattered nuclear light.

We show the $B - I$ map of Mkn 1066 in Fig. 10. Note that the I band nucleus is saturated, so the structure in the central few pixels is not real. The star forming regions in the host galaxy are clearly visible in Fig. 10. There is a very red region SW of the nucleus at 2.6″ (910 pc). Finally, there is a blue elongated structure NW of the nucleus (PA = 325°) with total extent 4.2″ (1.5 kpc). This structure agrees well with the axis of the [OIII] and radio emission, and possibly represents scattered light from the nucleus. Its colours are given in Table 1.

3.5. NGC 788

NGC 788 is an S0a galaxy at redshift $z = 0.0136$, with 1″ corresponding to 390 pc projected distance in the sky. We show its B band image of in Fig. 11. It shows faint spiral arms at ∼30″ (12 kpc) radius from the nucleus. The [OIII] emission extends to 4.3″ (1.7 kpc) from the nucleus at PA = 105°, while the major axis of the nuclear continuum is at PA = 112° (Mulchaey et al. 1996b).

We show $B - I$ maps of NGC 788 in Fig. 12 (the whole galaxy) and Fig. 13 (nuclear region). The blue inclined ring of emission with ∼30″ (12 kpc) radius around the nucleus, tracing the faint spiral structure is clearly visible in Fig. 12. The nucleus is situated between two blue regions (Fig. 13), the less extended at 0.4″ (160 pc) S (PA = 170°) and the more extended at 1.1″ (430 pc) NW (PA = 315°). There is also a red extended region at 1.3″ (510 pc) S–SW of the nucleus. Although the axis of the blue double structure (PA ∼ 150°) does not correspond well with the axis of the [OIII] emission (PA = 105°), the blue maxima may represent localized peaks in the scattered light from the nucleus. Their colours are given in Table 1.

3.6. NGC 5347

NGC 5347 is an SBab galaxy at redshift $z = 0.00778$, with 1″ corresponding to 230 pc projected distance in the sky. Its B band image is presented in Fig. 14. It shows a bar enclosed by a ring structure at ∼25″ (5.8 kpc) radius, and faint spiral arms emerging from the ring at the ends of the bar (see also Gonzalez-Delgado & Perez 1996). The bar is oriented roughly parallel to the major axis of the galaxy. The [OIII] emission of NGC 5347 has a double nuclear structure perpendicular to the bar (Pogge 1989). An Hα emission knot is located at 2.7″ (620 pc) NE at PA = 25° from the nucleus, perpendicular to the bar (Gonzalez-Delgado & Perez 1996). The knot has high excitation spectrum and a large Ca triplet EW, suggesting the presence of red supergiants associated with an old burst of star formation. The emission line ratios of the knot, however, indicate photoionisation by a hard AGN continuum (Gonzalez-Delgado & Perez 1996). The nuclear continuum emission is probably emitted anisotropically, as supported

by photon deficit arguments (Gonzalez-Delgado & Perez 1996).

We show the $B-I$ map of NGC 5347 in Fig. 15. The blue star forming regions, the ring structure and the spiral arms in the host galaxy are clearly visible. There is also a red dust lane running S of the nucleus roughly E to W at a closest distance of 3.3″ (760 pc), delineating the bar. In the central region, the emission knot at 2.7″ (620 pc) at PA = 25° NE of the nucleus is clearly seen. Even closer to the nucleus, there is a blue elongated structure with total extent ∼1.3″ (300 pc) toward N of the nucleus (PA = 10°). These structures probably represent the brightest localized peaks in the scattered light from the nucleus. Their colours are given in Table 1.

3.7. NGC 5929

NGC 5929 is an Sab pec galaxy interacting with the starburst galaxy NGC 5930, together forming the galaxy pair Arp 90. The redshift of NGC 5929 is $z = 0.00854$, with 1″ corresponding to 250 pc projected distance in the sky. The B band image of the system is shown in Fig. 16. NGC 5929 has a faint hard X–ray spectrum, implying heavy absorption (Rush & Malkan 1996). It has triple radio structure extended along PA = 61°, with total diameter 1.3″ (320 pc; Su et al. 1996). The SW lobe is at 0.7″ (170 pc) distance from the nucleus and is slightly stronger than the NE lobe at 0.6″ (150 pc) distance. The [OIII] emission resembles closely the radio morphology, with two peaks straddling the nucleus at PA ∼ 60° (Bower et al. 1994). However, the [OIII] peaks are closer to the nucleus (1.1″ = 280 pc separation). Also, the NE [OIII] component is bisected by a dust lane. The [OIII] emission does not define a clear biconical morphology as in many other Seyfert 2s. Also, there is no evidence for obscuration in the direct images, except the dust lane, nor do energy balance considerations suggest anisotropy of the nuclear radiation (Bower et al. 1994).

We show the $B-I$ maps of the whole system in Fig. 17 and of NGC 5929 in Fig. 18. There is a blue stellar tail from the N part of NGC 5929 toward NGC 5930 and a red bridge between the galaxies, probably stellar emission reddened by the disc of NGC 5930 (Fig. 17; see also Lewis & Bowen 1993). The nucleus of NGC 5929 (Fig. 18) is situated between two blue maxima at opposite sides of the nucleus, the closer and brighter at 0.8″ (200 pc) SW (PA = 225°) and the more distant and fainter at 2.0″ NE (PA = 45°). Since the orientation of this structure agrees well with the [OIII] and radio axes, and the peaks are only slightly further away from the nucleus than the respective [OIII] and radio peaks, they possibly represent extranuclear scattering mirrors of anisotropically escaping nuclear light. The colours of the blue maxima are given in Table 1. A very red region, probably due to dust emission, is located 3.4″ (850 pc) S of the nucleus (PA = 166°).

3.8. NGC 5953

NGC 5953 is an S0/a pec spiral galaxy at redshift $z = 0.00655$, with 1″ corresponding to 190 pc projected distance in the sky. It interacts with the late-type spiral NGC 5954, and together they form the galaxy pair Arp 91 (VV 244). We show a B band image of the system in Fig. 19. While NGC 5954 has pronounced spiral arms, faint emission to N and W of its disk and a stellar bridge extending toward NGC 5953, the latter appears relatively smooth. HI maps (Chengalur et al. 1995) show a long plume of emission to NW of NGC 5953, corresponding to faint optical stellar emission (Fig. 19), and probably associated to the S stellar bridge of NGC 5954.

From long–slit spectroscopy, Yoshida et al. (1993) detected an inclined ring of giant star forming regions around the nucleus of NGC 5953, with ring diameter ∼15″ (2.9 kpc). More recently, the circumnuclear star forming properties of NGC 5953 were studied by [OIII] and Hα imaging (Gonzalez-Delgado & Perez 1997) and by UV imaging (Colina et al. 1997). The UV continuum is concentrated in several compact circumnuclear knots in a ring with similar morphology to Hα. Yoshida et al. (1993) detected also a high–ionisation region 4″ (760 pc) NE from the nucleus at PA ∼ 50°. Its location agrees well with radio morphology (PA = 40°; Jenkins 1984), and it is probably ionised by an anisotropic nuclear continuum. Yoshida et al. estimate that the flux seen by the ENLR is an order of magnitude higher than that directly observed. The lack of similar emission region on the opposite (SW) side of the nucleus is probably due to obscuration and/or the torus inclination.

We show the $B-I$ maps of the whole system in Fig. 20 and of NGC 5953 in Fig. 21. The overall features already visible in the direct B band image (Fig. 19), such as the stellar bridge between the galaxies, and the long plume of emission to NW of NGC 5953, are even more clearly visible in the $B-I$ map (Fig. 20). In NGC 5953, the $B-I$ map (Fig. 21) clearly shows the inclined star forming ring oriented roughly N–S with diameter ∼ 13×8″ (2.5 × 1.5 kpc). There is a red arc around the nucleus E–N–W with two main peaks at 1.6″ (300 pc) at PA = 320°, and at 1.8″ (340 pc) at PA = 60°, inside the star forming ring. Finally, there is a faint narrow blue elongated structure of 0.5″ (100 pc) extent at PA = 220°. This elongation is at similar orientation to the [OIII] and radio axes and probably represent scattered light from the nucleus. Its colours are given in Table 1.

3.9. NGC 7212

NGC 7212 is in a pair of interacting galaxies. Its redshift is $z = 0.0266$, with 1″ corresponding to ∼770 pc projected distance in the sky. We show the B band image of NGC 7212 in Fig. 22. Polarised spectra of NGC 7212 show

broad components to Hα and Hβ, and this polarisation is higher than that in the continuum (Tran et al. 1992; Tran 1995a), an indication of a hidden BLR. Most likely, the polarisation arises from scattering by dust (Tran 1995a), because the spectrum is very red, the continuum polarisation rises smoothly to the blue, and the polarised flux spectrum is bluer than total flux spectrum. The [OIII] emission of NGC 7212 shows a jet-like high-ionisation feature extending up to 10″ (7.7 kpc) from the nucleus at PA = 10° (Tran 1995a). This jet is exactly parallel to the axis of the small scale double radio source (0.7″ separation; Falcke et al. 1998), and roughly perpendicular to the optical polarisation (PA = 93°), suggesting that the jet is collimated radiation from the hidden nucleus obscured by a torus. The line ratios of the jet indicate photoinisation by the nuclear continuum. There is a faint broad base to Hα, probably the BLR reflected from the obscured nucleus by an offnuclear scattering mirror. However, no obvious BLR component to NIR lines was found by Veilleux et al. (1997).

We show the $B-I$ maps of NGC 7212 in Fig. 23 (the whole system) and Fig. 24 (NGC 7212). The nucleus of NGC 7212 is very blue and an extended fan–shaped blue emission region extends from the nucleus to S (PA = 165°) with total extent 2.3″ (1.8 kpc). This blue region is bisected by a red dust lane. A much redder narrow dust lane is situated on the other side of the nucleus, at closest distance 3.7″ (2.8 kpc) at PA = 280°. Although the orientation of the blue elongation does not correspond perfectly with the [OIII] emission, it may represent scattered light from the nucleus. Its colours are given in Table 1.

3.10. NGC 7319

NGC 7319 (Arp 319) is an SBb galaxy belonging to the Stephen's Quintet compact group of galaxies. Its redshift is $z = 0.0225$, with 1″ corresponding to 650 pc projected distance in the sky. We show the B band image of NGC 7319 in Fig. 25. In the radio (van der Hulst & Rots 1981), NGC 7319 shows a jet-like feature SW to the nucleus at PA = 207° extending ∼6″ (3.9 kpc). The X–ray emission from Stephan's Quintet consists of two components: the soft X-ray emission probably arises from hot intracluster gas (Sulentic et al. 1995), while the hard X-ray emission, peaked on NGC 7319, is consistent with an absorbed powerlaw, and exhibits a strong Fe K line, providing strong evidence for an obscured nucleus in NGC 7319 (Awaki et al. 1997).

The [OIII] emission of NGC 7319 extends for ∼10″ (6.5 kpc) toward S–SW, possibly in the form of an ionisation cone (Aoki et al. 1996). The [OIII] morphology and PA agree well with the radio, however, the [OIII] peak is closer to the nucleus than the radio peak. The kinematics of the extended [OIII] emission indicates a high velocity outflow up to ∼9″ (5.8 kpc) from the nucleus, mainly photoionised by the nuclear radiation (Aoki et al. 1996). The number of ionising photons required to ionise the ENLR is over 10 times higher than the number of photons in our line of sight, strongly indicating an anisotropic nuclear radiation field (Aoki et al. 1996).

We show the $B-I$ map of NGC 7319 in Fig. 26. To the S of the nucleus (PA = 210°) there is a very red region at 0.7″ (460 pc), continuing further S as a more extended red region. The bluest region is situated 1.1″ (720 pc) N of the nucleus (PA = 10°). The orientation of the blue elongation agrees well with the [OIII] and radio axes, and probably represents scattered light from the nucleus. Its colours are given in Table 1.

4. Discussion

Unified models have recently received much emphasis in AGN research (see e.g. Antonucci 1993). These models postulate that the distinction between broad and narrow lined AGN is simply due to our viewing angle. All Seyferts have the same basic structure, but in Seyfert 2s the plane of a geometrically and optically thick dusty molecular torus lies close to our line of sight and it blocks our direct view of the nuclear source and the BLR. On the other hand, in Seyfert 1s we look along the axis of the obscuring torus, and directly see the nucleus.

Briefly, the evidence in favour of the unified models includes the detection in a growing number of Seyfert 2s of: **1)** polarised broad emission lines (e.g. Antonucci & Miller 1985; Miller & Goodrich 1990; Tran 1995b; Young et al. 1996), interpreted as scattered BLR emission by warm material above the torus (e.g. Krolik & Begelman 1988; Pier & Krolik 1992); **2)** broad NIR lines, revealing highly obscured BLRs (e.g. Blanco et al. 1990; Goodrich et al. 1994; Ruiz et al. 1994; Veilleux et al. 1997); **3)** the biconical geometry of the high excitation gas (e.g. Pogge 1989; Tadhunter & Tsvetanov 1989; Haniff et al. 1991; Wilson & Tsvetanov 1994; Mulchaey et al. 1996a), indicating that the ionizing nuclear radiation escapes anisotropically along the torus axis; **4)** large X–ray absorbing column densities and a strong Fe Kα emission line (e.g. Awaki et al. 1990; Matt et al. 1996; Malaguti et al. 1998); and **5)** a deficit of directly observed ionizing photons compared to that seen by the ENLR (e.g. Wilson et al. 1988; Kinney et al. 1991; Binette et al. 1993). The ENLR (cone) axis, the radio source (torus) axis and the optical nuclear continuum axis are usually significantly aligned with each other, while there is no correlation with the host galaxy axis at larger scales (e.g. Pogge & De Robertis 1993; Wilson & Tsvetanov 1994; Mulchaey & Wilson 1995; KW97; this paper).

The colour maps presented in this paper and in KW97 offer a new, independent method to test the unified models of AGN. What is the origin of the blue elongated or double structures visible in the colour maps of the circumnuclear regions of several Seyfert 2 galaxies? In Mkn

3, Mkn 573 and NGC 1068 (KW97), and Mkn 533, Mkn 607, Mkn 1066, NGC 5347, NGC 5929, NGC 5953 and NGC 7319 (this paper), these structures are closely parallel to the radio and ENLR emission (to within 20°). In the case of a *stellar bar*, we would expect *red* continuum colours from an old stellar population, clearly not seen. *Optical synchrotron emission* from the radio jets is also unlikely, because there is no detailed correspondence between the blue maxima and the radio structure, and the blue continuum is more extended than the radio continuum. Alternatively, the blue structures may be due to an *intrinsically extended nonstellar continuum*, e.g. emission from high velocity shock waves generated from the interaction of a radio jet with the ENLR gas (e.g. Sutherland et al. 1993). Such an extended component has been proposed to explain the constant Hβ EW over five decades of optical–UV continuum luminosity (Binette et al. 1993), and the larger polarisation of broad lines than continuum in many Seyfert 2s (Tran 1995b). However, a very close morphological correlation between the continuum and the high-velocity ionised gas is expected, but not seen in the colour maps.

Can any of the blue features be due to *star formation*? There is now increasing evidence for circumnuclear starbursts in many Seyfert 2 galaxies, e.g. strong far–IR and CO emission from cool dust (Heckman et al. 1989), strong extended mid-IR emission and spectral features from warm dust (Maiolino et al. 1995), and large NIR light-to-mass ratios (Oliva et al. 1995). Also, strong optical CaII triplet 8600 Å absorption with respect to weak MgI 5100 Å absorption (Cid Fernandes & Terlevich 1995), and UV spectral properties (Heckman et al. 1995) indicate that hot massive stars in a dusty metal-rich starburst can make a significant contribution to the nuclear optical/UV energetics of Seyfert 2s. In most Seyferts studied here, the blue elongations and double features are closely aligned with the linear radio structure and the emission line morphology. Although this could indicate that they are intrinsically blue regions of (jet–induced) star formation, we consider it unlikely because there is no direct evidence for star forming regions in the continuum images, and because the morphology of the regions is diffuse, unlike the sharp boundaries and knotty morphology usually seen in star forming regions. Furthermore, excitation maps indicate that the circumnuclear gas in Seyferts is mainly of high excitation, and does not originate from star formation (Mulchaey et al. 1996a). Finally, the detected polarised broad lines, heavily absorbed X-ray sources, strong Fe Kα lines and ionisation cones in an increasing number of Seyfert 2s argue for a hidden Seyfert 1 in them.

Therefore, the remaining and most attractive explanation for the blue features spatially coincident with the high-excitation circumnuclear gas is *scattering of the nuclear light* along the radio axis by dust or electrons (see also Pogge & De Robertis 1993; KW97). In either case the scattered continuum appears blue, but more so for dust scattering because of the wavelength dependence. The reason for the alignment between the continuum and the line emission in this case is that both the ionising and optical photons escape along the torus polar axis, and the optical continuum is scattered by dust and/or electron "mirrors" associated with the ionised gas. For most of the sample galaxies, the scattering is likely due to electrons, because of the shape of the polarised flux spectrum, the correlation of the Hβ luminosity with soft X-rays, and the strong Fe Kα emission and lack of low-energy X-ray absorption (Tran 1995b). However, dust is strongly favoured for Mkn 533, NGC 1068 and NGC 7212 (Tran 1995b; see also KW97). Note that the blue structures in Mkn 1, NGC 788 and NGC 7212 are only weakly aligned with the radio and ENLR axes (to within $20-40°$), and their relation with the scattering of the nuclear light remains uncertain.

Finally, in the context of unified models, we might expect to detect red regions across the nuclei associated with the dusty torus and perpendicular to the radio/ENLR axes (cf. red nuclear structures in NGC 5252 and Mkn 348; Kotilainen & Prieto 1995; Simpson et al. 1996). Such structures are clearly not seen in this sample. This can be understood if the true scale of the obscuring material is much smaller than our spatial resolution (as expected in the unified model; Mulchaey et al. 1996a). In that case, regions of low reddening will be included, and the nuclear reddening will be severely underestimated. Thus, while nuclear reddening may be important in Seyferts, it remains undetected because of the limited spatial resolution, while the larger scale dust lane features become visible, as in many objects of this sample. Indeed, if we were to detect reddening by dusty tori in the colour maps, these features would correspond to hundreds of pc of scale, much larger than expected in unified models.

5. Conclusions

Continuum colour maps provide a powerful method to reveal scattered nuclear light in the circumnuclear regions of Seyfert 2 galaxies. As in our previous paper (KW97), we have detected elongated or double blue morphological structures in the $B-I$ maps of several Seyfert 2 galaxies and found a good agreement with previous emission line and radio studies of these galaxies. In Mkn 533, Mkn 607, Mkn 1066, NGC 5347, NGC 5929, NGC 5953 and NGC 7319, we interpret the colour structure as arising from scattering of the nuclear continuum light from electrons or dust in extranuclear mirrors. In Mkn 1, NGC 788 and NGC 7212, the blue structures are less well in agreement with the radio and line emission, and their relationship with scattering regions remains uncertain. The colours of the blue maxima are consistent with those expected from scattering off dust or electrons, this conclusion strengthened by the combined sample of the two

papers in this series. Our findings thus strongly support the current unified models of AGN.

Acknowledgements. Thanks go to the referee, M. De Robertis, for several suggestions leading to the improvement of the figures, and to R. Falomo for advice in producing the final figures. This research has made use of the NASA/IPAC Extragalactic Database (NED), which is operated by the Jet Propulsion Laboratory, California Institute of Technology.

References

Antonucci R.R.J., 1993, ARA&A 31, 473
Antonucci R.R.J., Miller J.S., 1985, ApJ 297, 621
Aoki K., Ohtani H., Yoshida M., Kosugi G., 1996, AJ 111, 140
Awaki H., Koyama K., Kunieda H., Tawara Y., 1990, Nat 346, 544
Awaki H., Koyama K., Matsumoto H., et al., 1997, PASJ 49, 445
Binette L., Fosbury R.A.E., Parker D., 1993, PASP 105, 1150
Blanco P.R., Ward M.J., Wright G.S., 1990, MNRAS 242, 4P
Bower G.A., Wilson A.S., Mulchaey J.S., et al., 1994, AJ 107, 1686
Bower G.A., Wilson A.S., Morse J.A., et al., 1995, ApJ 454, 106
Chengalur J., Salpeter E.E., Terzian Y., 1995, AJ 110, 167
Cid Fernandes R., Terlevich R.J., 1995, MNRAS 272, 473
Colina L., Garcia Vargas M.L., Gonzalez-Delgado R.M., et al., 1997, ApJ 488, L71
De Robertis M.M., Shaw R.A., 1990, ApJ 348, 421
Falcke H., Wilson A.S., Simpson C., 1998, ApJ (in press)
Gonzalez-Delgado R.M., Perez E., 1996, MNRAS 280, 53
Gonzalez-Delgado R.M., Perez E., 1997, MNRAS 281, 781
Goodrich R.W., Veilleux S., Hill G.J., 1994, ApJ 422, 521
Haniff C.A., Ward M.J., Wilson A.S., 1991, ApJ 368, 167
Heckman T.M., Blitz L., Wilson A.S., Armus L., Miley G.K., 1989, ApJ 342, 735
Heckman T.M., Krolik J., Meurer G., et al., 1995, ApJ 452, 549 (H95)
Jenkins C.R., 1984, ApJ 277, 501
Kay L., 1994, ApJ 430, 196
Kinney A.L., Antonucci R.R.J., Ward M.J., Wilson A.S., Whittle M., 1991, ApJ 377, 100
Kotilainen J.K., 1998, MNRAS (submitted)
Kotilainen J.K., Prieto M.A., 1995, A&A 295, 646
Kotilainen J.K., Ward M.J., 1997, A&AS 121, 77 (KW97)
Krolik J.H., Begelman M.C., 1988, ApJ 329, 702
Kukula M.J., Pedlar A., Baum S.A., O'Dea C.P., 1995, MNRAS 276, 1262
Lewis J.R., Bowen D.V., 1993, MNRAS 264, 818
Maiolino R., Ruiz M., Rieke G.H., Keller L.D., 1995, ApJ 446, 561
Malaguti G., Palumbo G.G.C., Cappi M., et al., 1998, A&A 331, 519
Matt G., Fiore F., Perola G.C., et al., 1996, MNRAS 281, L69
Miller J.S., Goodrich R.W., 1990, ApJ 355, 456
Mulchaey J.S., Wilson A.S., 1995, ApJ 455, L17
Mulchaey J.S., Wilson A.S., Tsvetanov Z., 1996a, ApJ 467, 197
Mulchaey J.S., Wilson A.S., Tsvetanov Z., 1996b, ApJS 102, 309
Oliva E., Origlia L., Kotilainen J.K., Moorwood A.F.M., 1995, A&A 301, 55
Pier E.A., Krolik J.H., 1992, ApJ 401, 99
Pogge R.W., 1989, ApJ 345, 730
Pogge R.W., De Robertis M.M., 1993, ApJ 404, 563
Pogge R.W., De Robertis M.M., 1995, ApJ 451, 585
Ruiz M., Rieke G.H., Schmidt G.D., 1994, ApJ 423, 608
Rush B., Malkan M.A., 1996, ApJ 456, 466
Simpson C., Mulchaey J.S., Wilson A.S., Ward M.J., Alonso-Herrero A., 1996, ApJ 457, L19
Su B.M., Muxlow T.W.B., Pedlar A., et al., 1996, MNRAS 279, 1111
Sulentic J.W., Pietsch W., Arp H., 1995, A&A 298, 420
Sutherland R.S., Bicknell G.V., Dopita M.A., 1993, ApJ 414, 510
Tadhunter C., Tsvetanov Z., 1989, Nat 341, 422
Tran H.D., 1995a, ApJ 440, 578
Tran H.D., 1995b, ApJ 440, 597
Tran H.D., Miller J.S., Kay L.E., 1992, ApJ 397, 452
Ulvestad J.S., Wilson A.S., 1989, ApJ 343, 659
van der Hulst J.M., Rots A.H., 1981, AJ 86, 1775
Veilleux S., 1991, ApJ 369, 331
Veilleux S., Goodrich R.W., Hill G.J., 1997, ApJ 477, 631
Wilson A.S., Tsvetanov Z., 1994, AJ 107, 1227
Wilson A.S., Ward M.J., Haniff C.A., 1988, ApJ 334, 121
Young S., Hough J.H., Efstathiou A., et al., 1996, MNRAS 281, 1206
Yoshida M., Yamada T., Kosugi G., Taniguchi Y., Mouri H., 1993, PASJ 45, 761